ADVANCED OPTICAL MATERIALS
www.advopticalmat.de

Transient Structural Colors with Magnesium-Based Reflective Filters

*Peifen Lyu, Tao Gong, Mariama Rebello Sousa Dias, and Marina S. Leite**

Structural color filters have recently blossomed as a superior alternative to organic dyes or chemical pigments owing to their remarkable durability and compactness. With appropriate design, nanostructure-induced photonic or plasmonic resonance modes can give rise to either enhancement in transmission or suppression in the reflection within specific wavelength ranges in the optical regime, generating distinctive colors. However, the static optical properties due to fixed structural geometry and size after fabrication hinder their deployment in many cutting-edge technologies requiring adaptive complexion changes. Here, a multilayer thin film-based color filter incorporating Mg and MgO, earth-abundant and biodegradable materials, is devised. The devices display vivid hues spanning a broad gamut via the control of the film thickness. They also exhibit minimal color changes with varying angle views up to 40°–50°. Moreover, the tones fade away instantly upon immersion in water and then progressively transition to a different hue with the complete removal of the Mg-containing layers, realizing transient color responses. This approach holds great promise for alternative pixels with irreversible color-change capability as well as zero-power consumption and low cost, while making use of biodegradable materials.

1. Introduction

Color generation exploiting nanophotonics or plasmonic resonances (i.e., structural color generation) has been a burgeoning research arena with tremendous potential for a plethora of technological applications, such as image sensing, printing, optical information storage, and security tagging.[1–5] With the appropriate design of the size, shape, and materials for the used nanostructures, enhancement or inhibition of optical transmission or reflection within the visible wavelength regime can be induced on resonance, giving rise to the filtering of distinctive colors. Commonly used resonance structures include Fabry–Pérot (F–P) cavities,[6–9] plasmonic nanostructures,[10–14] and grating-coupled waveguides.[15–17] Compared with conventional approaches using organic dyes or chemical pigments, structural color filtering offers compelling advantages, including durability, environmental friendliness, high resolution, and compatible integration with monolithic fabrication.[2,18–20]

One fundamental constraint with those resonance structures is that the generated/filtered colors are static post-fabrication, yet varieties of modern technologies such as cryptography, data storage, and dynamic color display entail *on-demand* alteration or vanishment of hue. Although mechanisms to dynamically tailor the optical properties in resonance nanostructures have been well established via phase-changing materials,[21,22] electrical biasing/gating,[23–25] mechanical actuation or strain,[3,26,27] methods with lower power consumption and better cost-effectiveness are still called for. From material's perspective, structural color filters consist prevalently of conventional metals (e.g., Au, Ag, and Al) owing to their low optical loss. However, they are either nonearth abundant and CMOS-incompatible (Au, Ag) or non-biodegradable (Ag, Al), which often restricts their utilization in biosensing[28,29] and augmented reality.[30] Recently, magnesium (Mg) has drawn increasing research interest for nanophotonic and plasmonic applications as an earth-abundant, biodegradable, and CMOS-compatible alternative to conventional metals.[31–34] Besides, its optical property can be readily modified upon exposure to hydrogen or water, prompting its adoption in dynamic photonic devices.[9,35]

Here, we experimentally implement an Mg-based color-filtering multilayer structure based on two metal–insulator–metal (MIM) F–P cavities connected in tandem. Our devices visually exhibit multiple distinctive tints spanning the CMY reflective color gamut, verified by spectroscopic ellipsometry (SE)-measured reflection spectra featuring marked suppression at resonance wavelengths. We also find that the colors are insensitive to incident angles for most devices, which is a conducive characteristic for color display. In addition, we demonstrate that the colors can vanish within ≈40 s after immersion in water. The fast fading of hue is desirable for securing and protecting optical information as needed. Further, extending

P. Lyu, T. Gong, M. S. Leite
Department of Materials Science and Engineering
University of California
Davis, CA 95616, USA
E-mail: mleite@ucdavis.edu
T. Gong
Department of Electrical and Computer Engineering
University of California
Davis, CA 95616, USA
M. R. S. Dias
Department of Physics
University of Richmond
Richmond, VA 23173, USA
The ORCID identification number(s) for the author(s) of this article can be found under https://doi.org/10.1002/adom.202200159.

DOI: 10.1002/adom.202200159

the immersion time in water ultimately etches away the Mg-containing active layers, leaving behind the bottom cavity with a different reflective color due to a different resonance wavelength. Ultimately, our approach enables scalable, low-cost single-time color change with benign power consumption. Our material selection and their unique properties are suitable for applications where biodegradable materials are desired and irreversible color changes are needed. For instance, these pixels could be used as building blocks for biodegradable displays, where these components would disintegrate after stable operation. In health care, Mg-based structural colors could act as coatings of humidity-sensitive medical pills, where irreversible hue changes would indicate their exposure to high humidity levels. The non-toxic, green chemistry exploited represents a significant step towards the implementation of biodegradable and sustainable color sensors.

2. Reflective Color Filters

We propose an Mg-based thin-film reflective color filter, which features an irreversible shade transition in a low-cost (prices of metal ingots: Mg > US$ 7 kg^{-1}, Ag > US$ 800 kg^{-1}, Au > US$ 63 300 kg^{-1}, Al > US$ 3.5 kg^{-1}[36]) and all but power-free manner. **Figure 1** shows the schematic of our color-filtering structure and how the hue is changed. The optical devices are composed of seven layers of alternating metal and dielectric thin films. In essence, two MIM F-P resonance cavities are stacked together, separated by an MgO thin film (20-nm fixed thickness) to prevent potential interdiffusion of the metals. The top cavity consists of Mg (6 nm)-MgO-Mg (100 nm), while the bottom comprises Ag (30 nm)-Al_2O_3-Ag (100nm). The dielectric constants of the materials chosen are presented in Figure S1 (Supporting Information). Note that the dielectric properties of the top Mg layer behave differently from the bottom Mg likely due the increasing collision frequency of electrons in ultrathin films.[37,38] Experimentally, these layers are deposited in sequence using electron-beam evaporation (EBE). White light illuminated from the top is mostly reflected except around the resonance wavelength of the top cavity, which is determined by controlling the thickness of the middle dielectric layer. As such, a distinctive reflected color arises, provided the resonance falls into the visible wavelength regime. When the device is immersed in DI water (pH-neutral) for sufficient time, the top cavity that contains Mg and MgO dissolves as the result of reaction with water,[39] which exposes the bottom F–P cavity featuring a different hue.

Both Mg/MgO/Mg and Ag/Al_2O_3/Ag MIM stacks display tunable colors independently by tailoring the thickness of the middle dielectric layers based on Fabry–Pérot resonances,[1] as presented in **Figure 2**. Here, we show the photographs of five representative 1 cm^2 optical filters of each stack with MgO thickness from 54 to 156 nm and Al_2O_3 thickness from 97 to 169 nm in Figure 2a,d, respectively. The detailed characterization of each layer is listed in Tables S1 and S2 (Supporting Information) with a schematic of roughness as estimated and measured by ellipsometer in Figure S2 (Supporting Information). These ellipsometry models show good match with the cross-section TEM images in Figure S3 (Supporting Information), which validate the continuity of the ultra-thin top Mg layer. To quantify the optical responses of the structures, we measure the reflection spectra at 15° within the visible light wavelength range (360–830 nm). All samples are very stable in laboratory ambient conditions (relative humidity ≈ 33%), as evidenced by their similar optical response one day and eight months after fabrication presented in Figure 2b,e. In general, the increasing thickness of the dielectric layer shifts the reflection dips to a longer wavelength. To compare, the Mg/MgO/Mg stack (Figure 2b) tends to have a broader resonance than the Ag/Al_2O_3/Ag MIM (Figure 2e) due to the influence of ultrathin thickness of the top Mg and a higher ratio of roughness to metals on the surface.[10,7,40] The capping layer of native MgO on the top Mg (5–6 nm) dampens and broadens the resonance to a greater extent than the oxides on a 30 nm Ag layer. The difference of surface roughness between the stacks in Figure S4 (Supporting Information) even attenuates this effect. As a result, the Mg/MgO/Mg color filter can cover vivid hues on the border of the CYM range, while the hues produced by Ag/Al_2O_3/Ag are more concentrated in the center, as illustrated on the CIE 1931 space chromaticity diagrams, Figure 2c,f, respectively. Both filters display colors not achievable by the other. Therefore, a transient photonic device grouping these complementary pairs is expected to show the transition between distinctive hues.

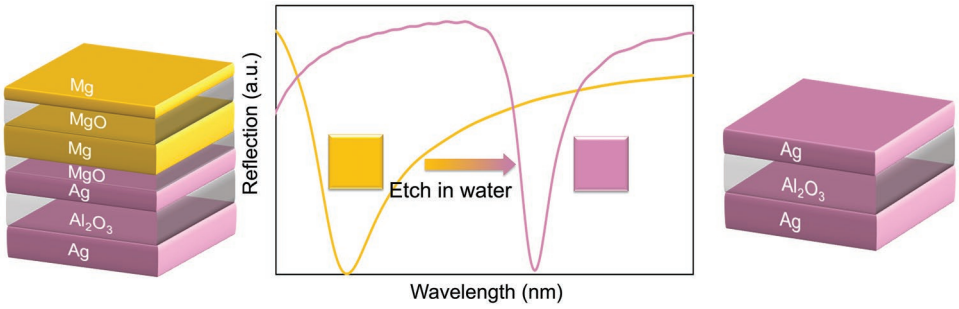

Figure 1. Schematic of color switching process using tandem MIM structures and selective etching. The device consists of seven thin-film layers. Both the bottom (magenta: Ag–Al_2O_3–Ag) and top (yellow: Mg–MgO–Mg) three layers constitute a metal–insulator–metal (MIM) stack, separated by a thin layer of the insulating layer (MgO) in between. After immersed in water, the Mg and MgO layers are etched, leaving the bottom MIM (pink) stack only. If the size of the insulating layers for the top and bottom stacks is chosen appropriately, the reflectivity of the device before and after etching features a reflection dip at selected wavelengths, enabling color change.

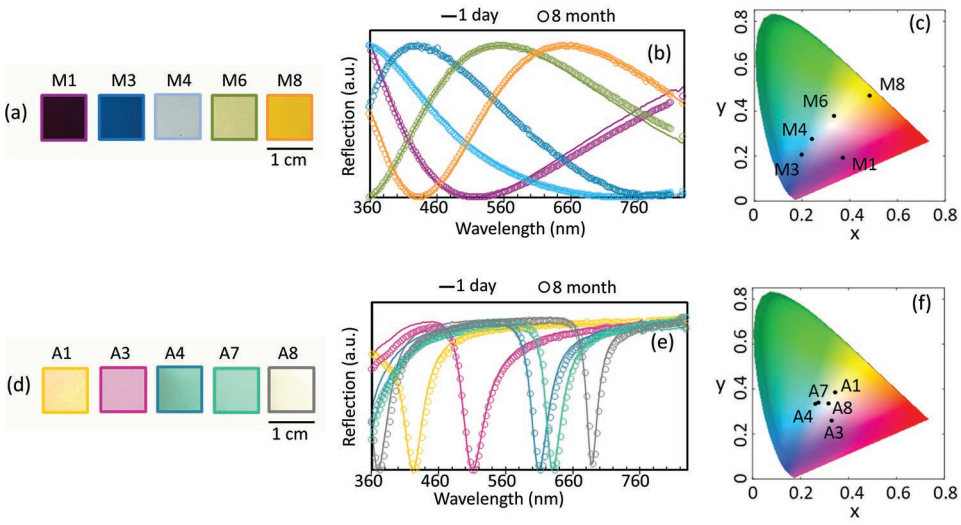

Figure 2. Structural pixels based on earth-abundant metals. Real-color photographs of pixels formed by a) 2 nm Mg/x nm MgO/100 nm Mg, where x = 54, 73, 94, 129, 156 nm, and by d) 25 nm Ag/y nm Al_2O_3/100 nm Ag, where y = 97, 125, 136, 159, 169 nm. The thickness of each layer is measured by spectroscopic ellipsometry (SE). b,e) Measured reflection at 15° as a function of wavelength for samples displayed in (a) and (d), respectively. Solid lines and dots refer to measurements acquired after one day and eight months of sample fabrication, respectively. c,f) CIE 1931 space chromaticity diagram with the fabricated color pixels from (a) and (d), respectively.

Figure 3 presents the reflection spectra (both calculated and measured) and photographs of four representative samples as a function of light incident angles. As expected, both Mg/MgO/Mg (M3, M8) and Ag/Al_2O_3/Ag (A3, A6) devices show shifts in their reflection dips towards shorter wavelengths as the incident angles increase from 15° to 80°. For stack M3 in Figure 3a, the vivid royal blue has persisted up to 40° and changed gradually to greyish brown at 70° and beyond, matching with the shift of reflection dips from 630 to 370 nm. Similar color transition behavior at various angles is also observed in stack M8 (Figure 3b) for a hue change from yellow (up to 40°) to grey (at 80°). As shown in Figure 3c, the originally magenta A3 pixel (reflection dip at 510 nm) fades into pink at 50°, and eventually reaches yellowish tan (reflection dip at 455 nm) at 80°. The color transition for stack A6 (see Figure 3d) is more dependent on the oblique angles undergoing from cyan to light green (20°–30°), to magenta (40°–60°) and finally rose pink at 80°, indicating a reflection dip shift of 70 nm. The angular-dependent chromaticity

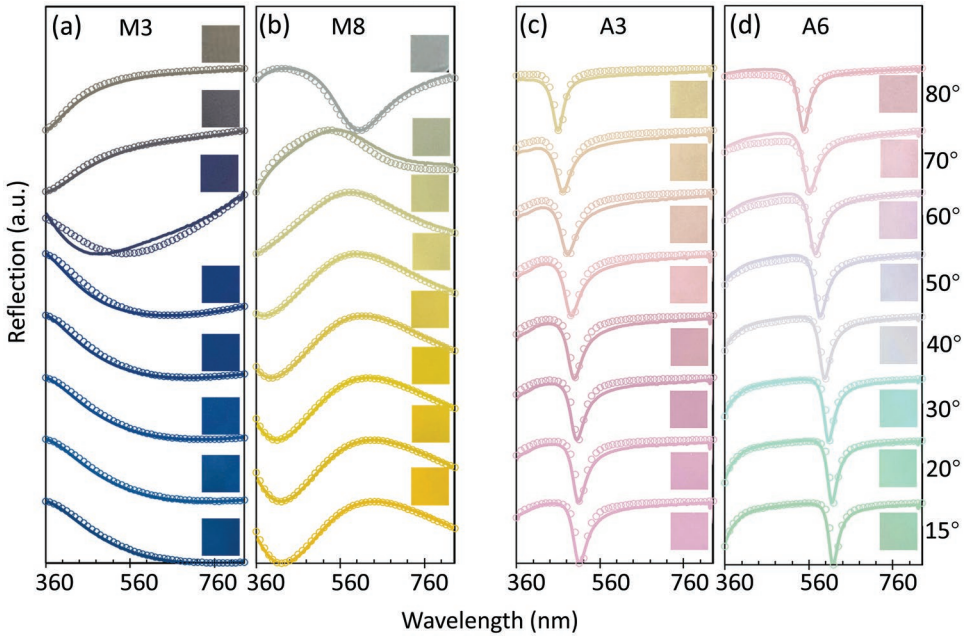

Figure 3. Angular dependence of chromaticity. Measured (solid lines) and calculated (open circles) reflection of MIM color filters for Mg-based structures with a) 73 nm and b) 146 nm of MgO, and with c) 125 nm and d) 150 nm of Al_2O_3. The orientation of the incident light is varied from 15° to 80°, as indicated. Insets: real-color photographs of the fabricated samples.

trend is also demonstrated in all the other MIM stacks we fabricated (see Figures S5 and S6, Supporting Information). This angular-dependent chromaticity arises from the interference of multiple reflections occurring inside the cavity of the MIM structure due to Fabry–Perot resonances. The sensitivity of the incident angle can be described in the equation below:[1]

$$\left|\frac{\Delta\lambda_r}{\Delta\theta}\right| \approx \frac{2d \cdot \sin\theta \cdot \cos\theta}{\sqrt{n^2 - \sin^2\theta}} \quad (1)$$

where $\Delta\lambda_r$ is the variation of the resonant wavelength, θ is the incident angle, n and d are the refractive index and thickness of the dielectric layer, respectively. According to this equation, the devices are insensitive to small incident angles (up to ≈40°), which is consistent with our observations for most samples. In addition, this sensitivity is directly proportional to the thickness of the cavity. Thus, higher dielectric spacer thickness enables higher angle-sensitivity. Although the overall consistent blue shift of reflection enables the system to cover more CYM gamut at high angles, most devices are insensitive to the position of view at low angles, which is desirable for applications in color display.

3. Transient Optical Behavior

Because both Mg and MgO are the primary materials responsible for the unique transient optical responses presented here, we immerse all the eight Mg/MgO/Mg color filters into ambient water (at room temperature and neutral pH) and confirm the fast shade transition is the result of reduced surface Mg layer (see supplementary video for the real-time experiment). Snapshots are presented in **Figure 4**a to show the color transition. In the first 20 s, the pixels quickly lose their vivid hues due to the reduced surface Mg layer (bubbles are produced through the gaps between the sample and holder while immersing in water). At 40 s, all hues vanish entirely, and the filters look similar to each other. Once the vivid hues disappear, the following color transition behavior is slower, as illustrated in Figure S7 (Supporting Information). After 80 min, all Mg-based layers are etched away without traceable byproducts. The remaining glass substrates are ready for reconfiguration. Figure 4b shows the change of chromaticity during the whole etching process from the vivid hues (black circles) before and eventually reaches the center (red triangle), representing the plain glass substrate, on the CIE 1931 color diagram. The calculated etching pathway based on simulated reflection spectra for reducing layer thickness from top to bottom materials in Figure S8 (Supporting Information) provides a more detailed visualization for color transition as the Mg/MgO/Mg stacks are exposed to water. The significant shift of hues caused by the removal of the top Mg layer confirms our previous prediction that the thin Mg layer (≈5–6 nm) on the top is responsible for the loss of vivid hue. This fast shade transition is valuable for the purpose of erasing sensitive information within seconds if needed and/or desired. In addition, the substrate left is reusable for other applications if desired.

To demonstrate the successful transient color changing behavior of the seven-layer transient photonic device, we choose two complementary pairs (M3-A6, A3-M8) to show the greatest contrast in color before and after etching in water. Through exposure to water, the top 4 layers, which consist of Mg and MgO, are expected to dissolve in water and leave the bottom Ag/Al_2O_3/Ag stack intact. The hue transitions in **Figure 5** take ≈1.5–2 h to reveal the second hue, which is slower than the fast vanishing of the original color presented previously. The M3-A6 stack displays royal blue at the beginning. Once immersed in water (at the ambient condition), the vivid color disappears within seconds, similar to the etching behavior for M3 in Figure 4a. After 10 min in water, the dark grey bottom Mg starts to show up while the top Mg and MgO slowly dissolve. Light green features are observed in the next 40 min as the remaining materials are etched away in a somewhat non-uniform manner. Small bubbles (H_2 gas) are observed as the byproduct of the reaction between Mg and water. These bubbles seem to exaggerate the surface

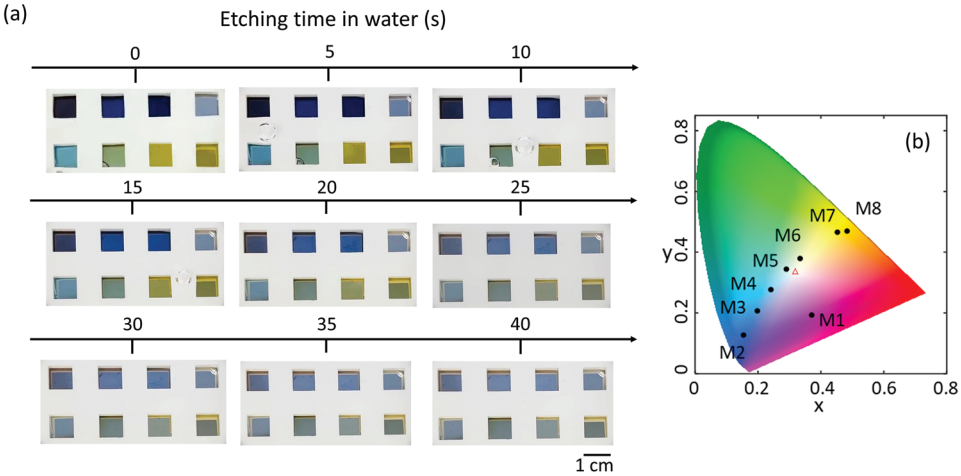

Figure 4. Mg-based color filters provide fast hue change. a) Photographs of Mg/MgO/Mg color filters as they dissolve in water, at room temperature, and neutral pH for the first 40 s. b) CIE 1931 space chromaticity diagram showing samples hue before (black circles) and after (red triangle) etching process.

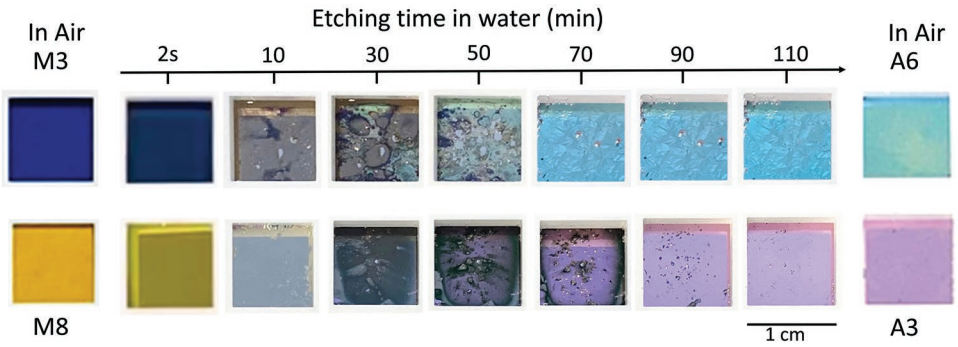

Figure 5. Real-time structural color change based on tandem MIM stack. Sequence of photographs showing full seven-layer Mg/MgO/Mg/MgO/Ag/Al_2O_3/Ag color pixels changing in hue from vivid royal blue to cyan (M3–A6) and from yellow to magenta (M8–A3), respectively, as the top Mg-based MIM structure is etched away by water, exposing the bottom Ag-based MIM filter.

roughness, making the structure look darkish instead of a mirror-like metallic surface. The final structure with cyan hue is successfully achieved after immersing in water for 70 min. After removing the optical device from the etching bath and drying it with N_2 gas, the bubbles are eliminated and leave a more uniform cyan filter, the same hue for an A6 stack in Figure S6 (Supporting Information). Similar transient hue change is applied to the M8-A3 stack to demonstrate the universality of the approach introduced here. The originally yellow pixel loses its vivid color within the first few seconds of etching and transfers gradually to magenta as the Mg and MgO dissolve in water for 110 min due to a thicker insulating layer, MgO. It is noticeable that the 20 nm connecting the MgO layer does not visually hinder the structure below, as confirmed in the calculated etching pathway in Figure S9 (Supporting Information). Thus, the seven-layer stacks are intentionally immersed in water for a longer time than the three-layer stacks in Figure 4 to ensure the complete etching of all Mg and MgO above. Through etching in water, our system enables one-time color tuning from the original hue of the top Mg/MgO/Mg stack to the second hue of the Ag/Al_2O_3/Ag stack in a zero-power manner without changing the materials itself, switching the light source or applying external power sources. The final state will persist since neither Ag nor Alumina is water-soluble and are both stable materials.

4. Conclusions

To summarize, we presented a new approach for transient, structural color switch based on multilayer thin films comprising Mg, an earth-abundant and biodegradable material. We demonstrated a wealth of vivid hues covering a broad color gamut by controlling the thicknesses of the incorporated F-P cavities. Meanwhile, the reflective tint variations with an incident angle for most of our devices are minimal at 40°–50°. These incident angle-agnostic reflections can favor their potential application in displays. Upon selective etching in water (at ambient conditions), the original shades fade promptly within ≈40 s, which is critical in information or data security technologies. In addition, the device color is entirely altered with sufficiently long immersion in water after the Mg-containing components are etched away. For example, we explicitly showed the irreversible color switching for the subtractive primary hues (i.e., cyan, magenta, yellow) in the CMY model, which forms the basis for reflective color filters. This single-time-tone switching process is easy to operate and highly scalable and may create new opportunities for next-generation biodegradable and low-cost color pixels and related technological applications. Moreover, our results solidify the transient photonics paradigm, where scalable and robust structural colors could be used to store and/or reveal sensitive information in situations where irreversible changes are required.

5. Experimental Section

Sample Fabrication: All the films were deposited by e-beam evaporation (AST Peva-600I at UC Berkeley Marvell Nanofabrication lab). Before deposition, the 1.0 cm^2 glass substrates were cleaned with acetone, 2-propanol, and deionized water, and then dried with N_2 gas. The deposition rates of Mg, MgO, Ag, and Al_2O_3 were about 2.2, 2.5, 2.0, and 2.7 Å s^{-1}, respectively. The layers in the color filters were deposited sequentially.

Dielectric Function Model and Thickness Characterization: The spectroscopic ellipsometer, J. A. Woollam M-2000 ellipsometer (from Center for Nano-Micro Manufacturing, CNM2 at UC Davis) was used to acquire reflection spectra at 55°, 65°, and 75° and transmission at normal incident plane within 193–1680 nm. The baseline measurements in air were taken before each transmission measurement. The dielectric functions of metals (on glass substrate) were fitted on CompleteEASE, the software coupled with the ellipsometer, considering both reflection and transmission measurement while models of oxides (on Si wafer) were based on reflection only. Furthermore, the dielectric constants obtained for each material by General Oscillator (Gen-Osc) models were used to determine the corresponding layer thickness in the multilayer stacks.

Angular-Dependent Reflection Measurements/Calculations: The experimental reflection spectra from 15° and 20° to 80° (in an increment of 10°) were measured by VASE ellipsometer from J. A. Woollam (at University of Richmond), using a light source with a wavelength range of 360–830 nm. The corresponding calculated reflections as a function of wavelength in 5 nm increments were simulated by the CompleteEASE software based on the fitted models consisting of dielectric functions and thickness for each stack.

Sample Etching Experiment: All color filters were loaded into a mechanical holder and immersed in deionized water at room temperature and neutral pH simultaneously. Videos were filmed to record and image the hue transition of the samples during the etching process.

Supporting Information

Supporting Information is available from the Wiley Online Library or from the author.

Acknowledgements

P.L. and T.G. contributed equally to this work. The authors acknowledge T. Deppe, Dr. K. Palm, and Dr. N. Hong (from J.A. Woollam) for fruitful discussions. M.S.L. thanks the National Science Foundation (Award No. 20-16617) for financial support. M.R.S.D. thanks the School of Arts and Sciences at the University of Richmond for funding. Part of this study was carried out at the UC Davis Center for Nano and Micro Manufacturing (CNM2). The authors acknowledge CNM2 at UC Davis and UC Berkeley Marvell Nanofabrication Laboratory for their infrastructure and technical assistance.

Conflict of Interest

The authors declare no conflict of interest.

Data Availability Statement

The data that support the findings of this study are available from the corresponding author upon reasonable request.

Keywords

color filters, earth-abundant materials, magnesium, structural colors, transient photonics

Received: January 22, 2022
Revised: April 2, 2022
Published online:

[1] C. Ji, K.-T. Lee, T. Xu, J. Zhou, H. J. Park, L. J. Guo, *Adv. Opt. Mater.* **2017**, *5*, 1700368.
[2] L. Shao, X. Zhuo, J. Wang, *Adv. Mater.* **2018**, *30*, 1704338.
[3] Y. Sun, L. Jiang, L. Zhong, Y. Jiang, X. Chen, *Nano Res.* **2015**, *8*, 406.
[4] N. J. Greybush, K. Charipar, J. A. Geldmeier, S. J. Bauman, P. Johns, J. Naciri, N. Charipar, K. Park, R. A. Vaia, J. Fontana, *ACS Nano* **2019**, *13*, 3875.
[5] A. Kristensen, J. K. W. Yang, S. I. Bozhevolnyi, S. Link, P. Nordlander, N. J. Halas, N. A. Mortensen, *Nat. Rev. Mater.* **2016**, *2*, 16088.
[6] Y.-T. Yoon, S.-S. Lee, *Opt. Express* **2010**, *18*, 5344.
[7] Z. Li, S. Butun, K. Aydin, *ACS Photonics* **2015**, *2*, 183.
[8] C. Yang, K. Mao, W. Shen, B. Fang, X. Fang, X. Zhang, Y. Zhang, X. Liu, *Appl. Phys. Lett.* **2016**, *109*, 241104.
[9] T. G. Farinha, C. Gong, Z. A. Benson, M. S. Leite, *ACS Photonics* **2018**, *6*, 272.
[10] T. G. Farinha, T. Gong, P. Lyu, E. Deniz, J. M. Hoerauf, M. S. Leite, *Opt. Mater. Express* **2021**, *11*, 1555.
[11] H. Wang, X. Wang, C. Yan, H. Zhao, J. Zhang, C. Santschi, O. J. F. Martin, *ACS Nano* **2017**, *11*, 4419.
[12] M. Miyata, H. Hatada, J. Takahara, *Nano Lett.* **2016**, *16*, 3166.
[13] T. D. James, P. Mulvaney, A. Roberts, *Nano Lett.* **2016**, *16*, 3817.
[14] J. Fontana, R. Nita, N. Charipar, J. Naciri, K. Park, A. Dunkelberger, J. Owrutsky, A. Piqué, R. Vaia, B. Ratna, *Adv. Opt. Mater.* **2017**, *5*, 1700335.
[15] A. F. Kaplan, T. Xu, L. J. Guo, *Appl. Phys. Lett.* **2011**, *99*, 143111.
[16] C.-H. Park, Y.-T. Yoon, S.-S. Lee, *Opt. Express* **2012**, *20*, 23769.
[17] M. J. Uddin, T. Khaleque, R. Magnusson, *Opt. Express* **2014**, *22*, 12307.
[18] Z. Yang, Y. Chen, Y. Zhou, Y. Wang, P. Dai, X. Zhu, H. Duan, *Adv. Opt. Mater.* **2017**, *5*, 1700029.
[19] E. Heydari, J. R. Sperling, S. L. Neale, A. W. Clark, *Adv. Funct. Mater.* **2017**, *27*, 1701866.
[20] V. R. Shrestha, S.-S. Lee, E.-S. Kim, D.-Y. Choi, *Nano Lett.* **2014**, *14*, 6672.
[21] M. Wuttig, H. Bhaskaran, T. Taubner, *Nat. Photonics* **2017**, *11*, 465.
[22] Y. Gutiérrez, P. García-Fernández, J. Junquera, A. S. Brown, F. Moreno, M. Losurdo, *Nanophotonics* **2020**, *9*, 4233.
[23] E. Arbabi, A. Arbabi, S. M. Kamali, Y. Horie, M. Faraji-Dana, A. Faraon, *Nat. Commun.* **2018**, *9*, 812.
[24] D. Franklin, Y. Chen, A. Vazquez-Guardado, S. Modak, J. Boroumand, D. Xu, S.-T. Wu, D. Chanda, *Nat. Commun.* **2015**, *6*, 7337.
[25] M. Huang, A. Jun Tan, F. Büttner, H. Liu, Q. Ruan, W. Hu, C. Mazzoli, S. Wilkins, C. Duan, J. K. W. Yang, G. S. D. Beach, *Nat. Commun.* **2019**, *10*, 5030.
[26] J. Y. Ou, E. Plum, L. Jiang, N. I. Zheludev, *Nano Lett.* **2011**, *11*, 2142.
[27] R. J. Suess, N. S. Bingham, K. M. Charipar, H. Kim, S. A. Mathews, A. Piqué, N. A. Charipar, *Adv. Mater. Interfaces* **2017**, *4*, 1700810.
[28] M. R. S. Dias, M. S. Leite, *Acc. Chem. Res.* **2019**, *52*, 2881.
[29] T. Gong, P. Lyu, K. J. Palm, S. Memarzadeh, J. N. Munday, M. S. Leite, *Adv. Opt. Mater.* **2020**, *8*, 2001082.
[30] S. Colburn, A. Zhan, A. Majumdar, presented at *Conf. Lasers and Electro-Optics*, San Jose, CA, June **2016**.
[31] J. Karst, M. Hentschel, F. Sterl, H. Linnenbank, M. Ubl, H. Giessen, *Opt. Mater. Express* **2020**, *10*, 1346.
[32] J. S. Biggins, S. Yazdi, E. Ringe, *Nano Lett.* **2018**, *18*, 3752.
[33] K. Appusamy, S. Blair, A. Nahata, S. Guruswamy, *Mater. Sci. Eng., B* **2014**, *181*, 77.
[34] X. Duan, N. Liu, *Acc. Chem. Res.* **2019**, *52*, 1979.
[35] J. Li, Y. Chen, Y. Hu, H. Duan, N. Liu, *ACS Nano* **2020**, *14*, 7892.
[36] T. Economics Markets of commodities, https://tradingeconomics.com/commodity (accessed: March 2022).
[37] G. Ding, C. Clavero, D. Schweigert, M. Le, *AIP Adv.* **2015**, *5*, 117234.
[38] M. Hövel, B. Gompf, M. Dressel, *Phys. Rev. B* **2010**, *81*, 035402.
[39] R. Li, S. Xie, L. Zhang, L. Li, D. Kong, Q. Wang, R. Xin, X. Sheng, L. Yin, C. Yu, Z. Yu, X. Wang, L. Gao, *Nano Res.* **2018**, *11*, 4390.
[40] H. Raether, *Thin Solid Films* **1975**, *28*, 119.

